International Journal of Recent Development in Engineering and Technology
Website: www.ijrdet.com (ISSN 2347-6435 (Online) Volume 15, Issue 06, June 2026)

Analysis and Flow Visualization of Thermally Affected Two-Layered Peristaltic Flow of Herschel–Bulkley Fluids

S. Kumarappa

Department of Mechanical Engineering, Bapuji Institute of Engineering and Technology, Davanagere, Karnataka, India.

***Abstract*—Peristaltic transport of a non-Newtonian fluid in a two-layered model is analytically investigated. The governing Navier–Stokes equations are formulated in cylindrical polar coordinates under the axisymmetric assumption. The flow consists of two incompressible viscous layers, with the fluid in the peripheral region modelled as a Herschel–Bulkley fluid and water occupying the core region. A sinusoidal peristaltic wave is imposed under the assumptions of low Reynolds number and moderate amplitude ratio. Closed-form analytical solutions are obtained to describe the velocity distribution, stream function, volumetric flux, limiting flux, and frictional force. The interface between the two layers is represented by a sixth-degree polynomial and solved numerically using the Newton–Raphson method. The analysis demonstrates the occurrence of positive pumping under both contraction and expansion waves. To validate the theoretical predictions, experimental studies are conducted, including flow resistance measurement, error estimation, and tube calibration. Numerical results are compared with existing studies, and computations are performed for both normal and heated fluids to examine the influence of temperature-induced viscosity variations. Flow visualization experiments are carried out under the long-wavelength approximation using dye and milk injection techniques. Theoretical streamlines are found to be in good agreement with experimental flow visualization, confirming the existence of positive pumping in both cases.**

***Keywords*— Peristaltic transport; Axisymmetric flow; Volumetric flux; Positive pumping**

I. INTRODUCTION

Peristaltic transport is a fundamental mechanism of fluid propulsion characterized by a progressive wave of contraction and expansion propagating along the walls of a flexible conduit. This traveling wave induces internal fluid motion without the need for an externally imposed pressure gradient. Unlike conventional pressure-driven flow, peristaltic motion relies on wall deformation to generate net transport, making it particularly suitable for handling sensitive, viscous, or heterogeneous fluids. The mechanism is self-sustained and capable of transporting fluids even against adverse pressure gradients, thereby distinguishing it from traditional pumping processes.

Peristaltic transport is widely observed in biological systems. It governs the movement of food bolus through the gastrointestinal tract, the transport of urine from the kidneys to the bladder via the ureters, and the propulsion of chyme within the intestines. Similar mechanisms are employed in biomedical devices such as heart–lung machines, dialysis pumps, and controlled drug delivery systems, where contamination-free and precisely regulated pumping is essential. Beyond biomedical applications, peristaltic principles are increasingly utilized in microfluidic devices, chemical processing systems, and soft robotic actuators. Owing to this broad spectrum of applications, peristaltic motion continues to attract sustained interest in applied mathematics, fluid mechanics, biomechanics, and bioengineering.

From a theoretical standpoint, peristaltic motion is commonly analysed under the long-wavelength approximation and low Reynolds number assumption. In the long-wavelength limit, the characteristic wavelength of the traveling wave is much larger than the channel radius, causing axial variations to dominate radial variations. The low Reynolds number condition ensures that viscous forces significantly outweigh inertial forces, which is typical in physiological flows and microscale transport systems. Under these simplifying assumptions, the governing Navier–Stokes equations reduce to a more tractable form, enabling analytical evaluation of velocity profiles, pressure gradients, volumetric flow rate, stream function, and flow resistance.

These classical formulations provide fundamental insight into the pumping mechanism. They demonstrate that mean transport arises from the nonlinear interaction between forward flow in the central core region and reverse flow near the channel walls. This interaction leads to important flow phenomena such as reflux, trapping (formation of internally circulating bolus-like zones), and net pressure generation even in the absence of externally applied pressure differences. Analytical investigations in both planar and axisymmetric geometries have shown that wave amplitude, shape, and propagation speed strongly influence pumping efficiency and pressure characteristics.

Despite this well-established mathematical foundation, most classical models assume Newtonian fluid behavior and isothermal conditions. In practical situations, however, many transported fluids exhibit complex rheological properties. Biological fluids such as blood, synovial fluid, and mucus display non-Newtonian behaviour, including yield stress and shear-dependent viscosity. These characteristics significantly affect velocity distribution, wall shear stress, and energy dissipation. Furthermore, in thermally sensitive systems, viscosity varies with temperature, introducing additional coupling between thermal and momentum transport mechanisms.

An additional complexity arises from layered flow configurations frequently encountered in physiological transport. For instance, microcirculatory flows may consist of distinct core and peripheral regions due to variations in cell concentration and rheological properties. Such layered structures influence interface dynamics, shear stress distribution, and overall pumping performance. Classical single-layer models are therefore insufficient to accurately describe these multi-region systems.

Consequently, there is a strong need to develop advanced mathematical models that incorporate thermo-rheological coupling, non-Newtonian constitutive behaviour, layered flow dynamics, and rigorous interface determination. Comprehensive formulations of this nature are essential for accurately predicting peristaltic transport under physiologically and industrially relevant conditions. By integrating realistic rheology, thermal effects, and layered configurations, modern peristaltic flow analysis can provide deeper insight into complex transport phenomena and support the improved design of biomedical and microfluidic pumping systems.

II. Literature Review

Peristaltic transport has been extensively investigated since the seminal work of Shapiro et al. [1], who developed the classical long-wavelength, low-Reynolds-number model for viscous flow induced by sinusoidal wall motion. Their analytical formulation established the fundamental relationship between pressure rise and volumetric flow rate and remains the cornerstone of peristaltic flow theory. Earlier work by Fung and Yih [2] provided additional insight into the mechanics of peristaltic motion in deformable conduits, emphasizing nonlinear wall deformation effects.

The extension of peristaltic theory to physiological fluids was pioneered by Srivastava et al. [3], who modelled blood as a two-layer Casson–Newtonian fluid system. Their results demonstrated that the peripheral plasma layer significantly influences pressure–flow characteristics and wall shear stress distribution. Siddiqui and Schwarz [4] further incorporated second-order non-Newtonian effects, showing that fluid elasticity alters velocity distribution and pumping performance.

Subsequent developments focused on generalized Newtonian and viscoelastic fluids. Rajagopal and Gupta [5] analysed non-Newtonian peristaltic transport and highlighted the role of rheological parameters in modifying pressure gradients. Selverov and Stone [6] investigated peristaltically driven microchannel flows, demonstrating enhanced mixing performance under moderate wave amplitudes. Vajravelu et al. [7] incorporated heat transfer effects in Jeffrey fluid transport through porous media, establishing the strong coupling between thermal gradients and flow behaviour.

Incorporation of magnetic fields and electromagnetic effects marked a significant advancement in modelling. Abd-Alla et al. [8] examined magnetohydrodynamic (MHD) peristaltic transport of Jeffrey fluids and showed that Lorentz forces reduce velocity magnitude while increasing pressure rise. Similarly, Hafez et al. [9] studied dusty fluid transport under thermal effects and demonstrated complex interactions between particle concentration and heat transfer.

The influence of variable fluid properties and activation energy models was addressed by Rafiq et al. [10], who reported that temperature-dependent viscosity significantly modifies velocity profiles and trapping limits. Gudekote et al. [11] analysed Eyring–Powell fluid transport under MHD influence and showed that non-Newtonian rheology enhances pumping efficiency under specific Hartmann numbers. Nadeem and Akbar [12] extended the framework to nanofluids, indicating improved thermal performance in biomedical transport systems.

Electroosmotic slip mechanisms were incorporated by Ellahi et al. [13], revealing that surface charge effects and electric fields substantially influence pressure rise and volumetric flux. Riaz et al. [14] analysed thermal radiation effects in peristaltic nanofluid transport and reported enhanced heat transfer rates under radiative flux conditions.

Recent investigations (2020–2025) have emphasized hybrid nanofluids, entropy generation, slip boundary conditions, and temperature-dependent viscosity models. Singh and Shah [15] demonstrated enhanced pumping of blood under non-Newtonian assumptions. Vernekar et al. [16] examined villi-patterned channel hydrodynamics, connecting peristaltic transport theory with gastrointestinal biomechanics.

Henn and Alim [17] analysed viscosity-dependent nutrient uptake mechanisms, providing interdisciplinary biological validation.

Hybrid nanofluid models were further explored by Sohail et al. [18], while Hayat et al. [19] investigated third-grade nanofluid behaviour. Rashidi et al. [20] studied entropy generation in MHD peristaltic systems, identifying optimal thermodynamic operating conditions. Slip effects and porous media influence were addressed in [21]–[23], confirming that permeability and wall slip significantly modify wall shear stress.

More recent works [24]–[30] examined convective heat transfer, electroosmotic effects, Carreau and third-grade fluids, and temperature-dependent viscosity models. Khan et al. [30] and Raza et al. [35] specifically demonstrated that viscosity variation with temperature leads to nonlinear changes in frictional force and pumping characteristics. Axisymmetric geometries and hybrid MHD nanofluid models were developed in [31]–[34], showing improved agreement between theoretical and experimental predictions.

Although substantial theoretical progress has been achieved, comprehensive models that simultaneously incorporate layered non-Newtonian rheology, temperature-dependent viscosity, axisymmetric geometry, and experimental validation remain limited. The present study aims to address this gap by integrating thermo-rheological coupling with layered flow structures to better predict frictional force and pumping performance in peristaltic transport systems.

II.A. Research Gap and Objectives of the Present Study

The following research gaps are identified:

1. Temperature-dependent viscosity effects in peristaltic transport have not been systematically incorporated into two-layer non-Newtonian models, despite their relevance to physiological and experimental flows.
2. Herschel–Bulkley fluid models, which unify yield stress and shear-dependent viscosity, are rarely employed in axisymmetric layered peristaltic transport.
3. Interface dynamics between core and peripheral layers are often assumed a priori; rigorous determination via higher-order polynomial formulations and numerical solution techniques is scarce.
4. Combined analytical–experimental studies, particularly those employing flow visualization to validate streamlines, trapping, and positive pumping, are limited in the literature.
5. Limiting flux and friction force analyses under simultaneous variations of viscosity ratio, amplitude ratio, and temperature have not been comprehensively reported.

Accordingly, the present study develops an analytical model for peristaltic transport of a two-layered Herschel–Bulkley fluid in an axisymmetric tube under long-wavelength and low Reynolds number approximations. The governing equations are formulated in cylindrical coordinates, the interface position is determined numerically, and the effects of temperature-induced viscosity variation on velocity, stream function, volumetric flux, limiting flux, and friction force are quantified. The theoretical predictions are validated through experimental flow visualization, providing a comprehensive applied mathematical framework for temperature-sensitive layered peristaltic transport.

To address these gaps, the present work develops an analytical model for peristaltic transport of a two-layered Herschel–Bulkley fluid in an axisymmetric tube, incorporating temperature-dependent viscosity effects. The interface between the layers is determined numerically using a polynomial formulation, and key flow parameters—including velocity, stream function, volumetric flux, limiting flux, and friction force—are evaluated. The analytical results are further supported by experimental flow visualization, enabling direct comparison between theoretical predictions and observed flow behavior. This combined approach provides a more comprehensive understanding of positive peristaltic pumping in thermally influenced, layered non-Newtonian flows.

II.B. Objectives of the Project

The primary objectives of the present study are as follows:

- To develop an analytical model for peristaltic transport based on the Navier–Stokes equations in cylindrical polar coordinates under the assumptions of low Reynolds number and long-wavelength approximation.
- To numerically evaluate key flow characteristics, including velocity distribution, pressure variation, volumetric flux, limiting flux, and time-averaged mean flow (flow resistance) under different thermal conditions.
- To determine the stream function and time-averaged volumetric flux by numerically solving a sixth-degree polynomial equation governing the interface between the core and peripheral layers.

International Journal of Recent Development in Engineering and Technology
Website: www.ijrdet.com (ISSN 2347-6435 (Online) Volume 15, Issue 06, June 2026)

- To analyse and compare the flow rates in the core and peripheral regions for varying viscosity ratios.
- To investigate the influence of temperature-dependent viscosity on peristaltic transport under normal and heated fluid conditions.

The study aims to establish a mathematical framework for analysing peristaltic transport of a two-layered non-Newtonian fluid in an axisymmetric tube, with particular emphasis on thermo-rheological coupling and pumping efficiency.

II.C. Methodology

- Formulation of the governing Navier–Stokes equations in cylindrical polar coordinates under low Reynolds number and long-wavelength approximations.
- Consideration of a two-layer fluid configuration consisting of a core layer and a peripheral layer with distinct viscosities.
- Representation of the interface between the two layers using a sixth-degree polynomial, solved numerically to satisfy continuity and mass conservation conditions.
- Numerical computation of velocity distribution, pressure rise, stream function, volumetric flux, limiting flux, and time-averaged mean flow (flow resistance).
- Comparative analysis under normal and heated conditions to account for temperature-induced viscosity variations.

The velocity profiles, pressure rise, and flow rates in both layers are quantitatively characterized for varying thermal conditions. Limiting flux and frictional resistance are determined as functions of amplitude ratio and viscosity ratio. Conditions leading to positive peristaltic pumping with reduced frictional losses are identified. The study further provides enhanced insight into the influence of temperature-dependent viscosity on two-layered peristaltic transport, supported by numerical evaluation of stream function and time-averaged flux.

III. Experimental Flow Visualisation

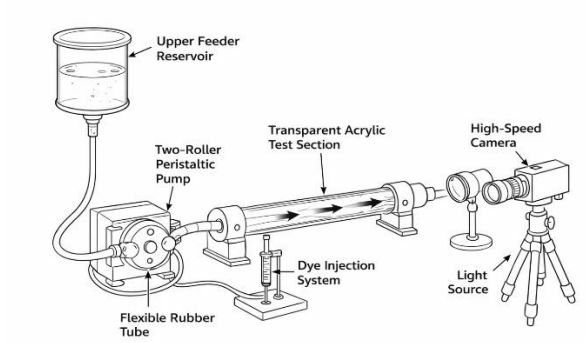

Figure III.A.: Schematic diagram of the experimental setup for peristaltic flow visualisation

The experimental arrangement employed for peristaltic flow visualisation is schematically illustrated in Figure III.A. The setup consists of a two-roller peristaltic pump positioned between an upper feeder reservoir and a lower collector reservoir, forming a closed-loop fluid transport system. The pump induces peristaltic motion by periodic compression and relaxation of a flexible tube, thereby generating a traveling contraction wave responsible for fluid propulsion.

The working fluid is conveyed through a flexible rubber tube of inner diameter 10.0 mm and wall thickness 1.5 mm, which is mechanically compatible with the peristaltic rollers. This rubber tube is connected downstream to a transparent acrylic tube, which serves as the test section for flow visualization. The transparency of the acrylic tube enables direct optical access to the flow field without disturbing the peristaltic motion.

A syringe-based dye injection system is mounted near the junction of the rubber tube and the acrylic test section. This location is selected to ensure that the injected tracer enters a region of fully developed peristaltic flow. Dye injection is carried out carefully to avoid perturbation of the base flow. A high-speed camera equipped with a zoom lens is mounted vertically above the test section to capture time-resolved images of the evolving flow patterns. The camera alignment ensures that the tube axis coincides with the imaging plane, enabling accurate qualitative assessment of flow structures.

International Journal of Recent Development in Engineering and Technology
Website: www.ijrdet.com (ISSN 2347-6435 (Online) Volume 15, Issue 06, June 2026)

The rotational speed of the peristaltic pump motor is regulated using a variable DC power supply. For all visualization experiments, the motor speed is adjusted such that a steady, fully developed peristaltic flow is established before image acquisition. The rotating rollers generate a traveling sinusoidal deformation of the tube wall, which produces axial transport of discrete fluid elements along the tube length.

Flow visualization is performed by injecting tracer dyes of different colors (red, blue, and black), as well as milk, into the test section. The evolution of the dye streaks provides qualitative insight into the underlying flow characteristics, including streamline patterns, axial velocity distribution, trapping phenomena, and regions of reflux. The choice of multiple tracers facilitates clear visualization of flow paths and enhances contrast under varying temperature and flow conditions.

All visualization experiments are conducted at a constant volumetric discharge of 140 ml/min to maintain consistency across different test conditions. In addition to dye injection, small neutrally buoyant immiscible fluid blocks are introduced into the flow to examine localized transport behaviour, bolus formation, and particle-like motion within the peristaltic wave. These blocks enable observation of flow segmentation and the extent of axial displacement during successive wave cycles.

The experimentally observed flow patterns are compared qualitatively with theoretical predictions obtained from the analytical model. A close agreement is observed in terms of streamline distribution, trapping regions, and overall positive pumping behavior. The visualization results thus provide experimental validation of the mathematical model and support the theoretical conclusions regarding peristaltic transport characteristics under low Reynolds number and long-wavelength conditions.

IV. Results And Discussions

IV.A. Formulation

The flow induced by an infinite train of peristaltic waves is assumed to be periodic and dynamically equivalent to that generated by a single sinusoidal wave propagating along the tube wall. Owing to this periodic nature, the physical domain can be reduced to a finite computational region corresponding to one wavelength.

In the present study, peristaltic motion is generated experimentally using a peristaltic pump, producing a sequence of identical waves that satisfy the no-slip condition at the tube wall, consistent with the measured peristaltic operating parameters.

The working fluid is modelled as a non-Newtonian Herschel–Bulkley fluid, and the flow is assumed to occur through a circular tube of radius ‘a’. The governing equations are derived from the Navier–Stokes equations formulated in cylindrical polar coordinates. The analysis is carried out under low Reynolds number conditions, with negligible inertial and body forces and dominant viscous effects, which are appropriate for physiological as well as laboratory-scale peristaltic transport.

Peristaltic motion is imposed by prescribing a sinusoidal wave of constant speed ccc traveling along the tube wall. The fluid domain is considered to be two-layered, comprising an inner core layer and an outer peripheral layer, each characterized by distinct Herschel–Bulkley rheological parameters. This layered representation enables the model to incorporate yield stress effects together with shear-thinning or shear-thickening behaviour in a unified mathematical framework.

The wave speed ‘c’ is selected based on physiological relevance and experimental operating conditions. The resulting formulation provides the foundation for evaluating the velocity distribution, pressure gradient, volumetric flux, limiting flux, and related flow characteristics of two-layered peristaltic transport, including the influence of temperature-dependent viscosity.

To formulate the peristaltic transport of the fluid in a cylindrical tube, the following assumptions are made:

- Peristaltic waves are progressive and sinusoidal in nature.
- An integral number of wavelengths exists between the two reservoirs.
- The pressure difference between the reservoirs remains constant.
- The flow is inertia-free (low Reynolds number regime).
- The wall slope is sufficiently small to be neglected.
- The amplitude ratio is chosen arbitrarily within the admissible range.
- Temperature effects are incorporated through viscosity variation in the analysis.

International Journal of Recent Development in Engineering and Technology
Website: www.ijrdet.com (ISSN 2347-6435 (Online) Volume 15, Issue 06, June 2026)

The following mathematical analysis is presented below.

IV.A.i. Velocity with respect to Temperature

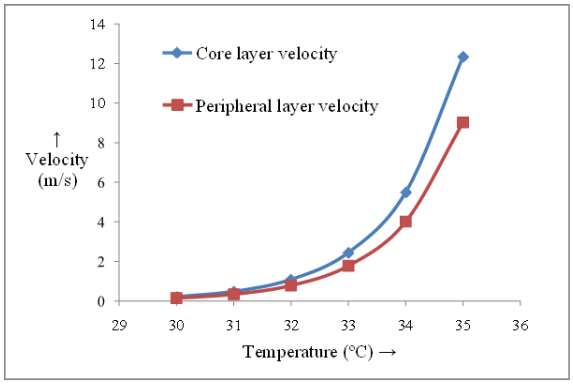

Fig IV.A.i.: Variation of Velocity with respect to Temperature

Fig. IV.A.i.. illustrates the variation of axial velocity with respect to temperature for the peristaltic transport under consideration. It is observed that an increase in temperature leads to a corresponding increase in fluid velocity across the flow domain. This behaviour is attributed to the reduction in fluid viscosity at elevated temperatures, which lowers viscous resistance and enhances momentum transport. Consequently, the velocity profiles become steeper, with higher peak velocities occurring near the tube centreline. The figure highlights the significant influence of thermal effects on the flow dynamics and confirms that temperature-dependent viscosity plays a crucial role in regulating peristaltic transport characteristics.

I*V.A. ii. Total flow rate with respect to Temperature*

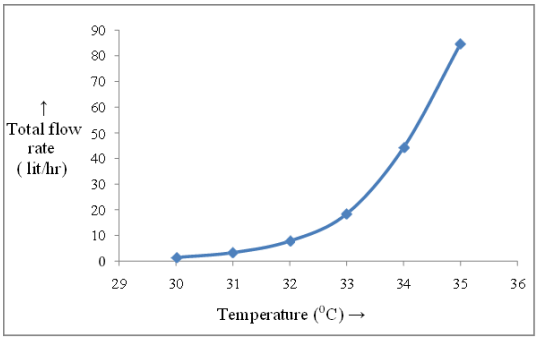

Fig. IV.A.ii.: Variation of Total flow rate with respect to Temperature

Fig. IV.A. ii. shows the variation of the total volumetric flow rate with respect to temperature for the peristaltic transport. It is observed that the total flow rate increases monotonically with an increase in temperature. This enhancement in flow rate is primarily due to the decrease in fluid viscosity at higher temperatures, which reduces the viscous resistance offered to the peristaltic motion. As a result, the pumping efficiency improves and a larger volume of fluid is transported for the same wave and operating conditions. The figure clearly demonstrates the strong coupling between thermal effects and peristaltic pumping performance, emphasizing the importance of temperature-dependent rheological properties in accurately predicting flow behaviour.

IV.A.iii. Time averaged flux with respect to Temperature

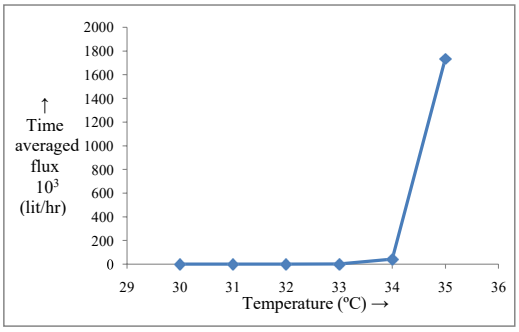

Fig. IV.A..iii.: Variation of Time averaged flux with respect to Temperature

Fig. IV.A.iii**.** illustrates the variation of the time-averaged volumetric flux with respect to temperature for the peristaltic transport. It is evident from the figure that the time-averaged flux increases as the temperature rises. This behaviour is attributed to the reduction in fluid viscosity with increasing temperature, which weakens viscous damping and enhances the net forward transport induced by the peristaltic wave. Consequently, the contribution of positive pumping becomes more pronounced at elevated temperatures, leading to higher mean flux values over a wave period. The results highlight the significant influence of thermal effects on the long-term transport characteristics of peristaltic flow

International Journal of Recent Development in Engineering and Technology
Website: www.ijrdet.com (ISSN 2347-6435 (Online) Volume 15, Issue 06, June 2026)

IV.A.iv. Flow rate in core layer with respect to Interface

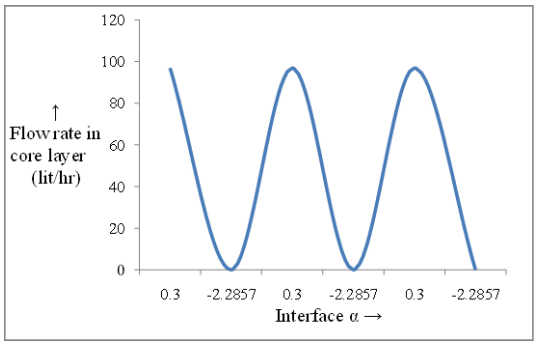

Fig IV.A.iv.: Variation of Flow rate in core layer with respect to Interface

Fig. IV.A.iv. depicts the variation of the volumetric flow rate in the core layer with respect to the interface position. It is observed that the core-layer flow rate is strongly influenced by the location of the interface separating the core and peripheral layers. As the interface shifts outward, resulting in an increase in the effective core radius, the flow rate in the core layer increases due to the larger cross-sectional area available for transport and the reduced influence of peripheral-layer resistance. Conversely, an inward shift of the interface leads to a reduction in core-layer flow rate. The figure highlights the sensitivity of layered peristaltic transport to interface dynamics and underscores the importance of accurately determining the interface position in two-layer fluid models.

IV.A. v. Pressure gradient with respect to Amplitude ratio

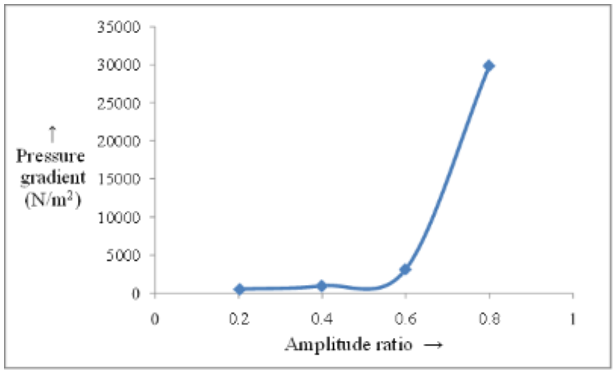

Fig IV.A.v..: Variation of Pressure gradient with respect to Amplitude ratio

Fig. IV.A.v.. illustrates the variation of the axial pressure gradient with respect to the amplitude ratio of the peristaltic wave. It is observed that the magnitude of the pressure gradient increases with an increase in amplitude ratio, indicating stronger wall deformation and enhanced resistance to flow in the constricted regions of the tube. Larger amplitude ratios lead to more pronounced contraction and expansion of the tube walls, thereby intensifying viscous effects and requiring a higher-pressure gradient to sustain the flow. This behaviour confirms the significant role of wave amplitude in controlling the pumping efficiency and pressure characteristics of peristaltic transport under low Reynolds number conditions.

IV.A.vi. Friction force at the wall (F)

The fluid particles describe the internal changes in their characteristics when the fluid temperature is solving increasing leads to change in the viscosity and stress at the wall. As a result, the friction among the particles, it is modeled as the area of the frictional force exists at the inner wall.

IV.A.vi. (a) Friction force at the wall with respect to Temperature

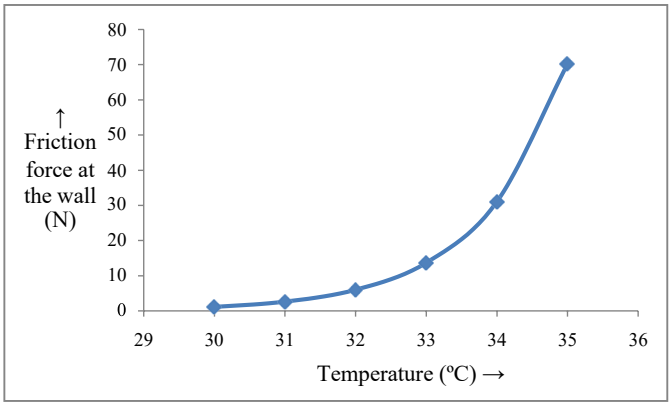

Fig IV.A.vi. (a): Variation of Friction force at the wall with respect to Temperature

Fig. IV.A.vi. (a) illustrates the variation of frictional force F with lubricating oil temperature T_L in the range of 30–35 °C, explicitly accounting for temperature-dependent viscosity. It is observed that the frictional force increases rapidly with increasing temperature, rising from 1.0240 N at 30 °C to 70.1061 N at 35 °C, indicating a strongly nonlinear thermal response.

International Journal of Recent Development in Engineering and Technology
Website: www.ijrdet.com (ISSN 2347-6435 (Online) Volume 15, Issue 06, June 2026)

As the lubricating oil temperature increases, the viscosity becomes a function of temperature and varies significantly within the operating range. The temperature-dependent viscosity alters the velocity gradients and shear stress distribution at the fluid–wall interface. Under the imposed mechanical driving conditions, this variation in viscosity leads to enhanced shear stresses, resulting in a substantial increase in frictional force. The nonlinear growth of friction reflects the combined influence of thermal effects and viscous dissipation within the flow field.

These results emphasize that temperature-dependent viscosity plays a critical role in governing frictional resistance and must be incorporated into theoretical and experimental models for accurate prediction of peristaltic and lubrication-driven transport systems.

IV.A. vi. (b) Variation of Friction force at the wall with respect to Temperature

When the fluid is heated to temperatures of 30, 31, 32, 33, 34, 35, 40, 43, and 45 °C, the distinction between the core layer and the peripheral layer progressively diminishes. As a result, the two-layered flow configuration effectively reduces to a single-layer flow regime. Under these conditions, the properties of the core layer become identical to those of the peripheral layer, i.e., Core layer=Peripheral layer ⇒Single-layer flow

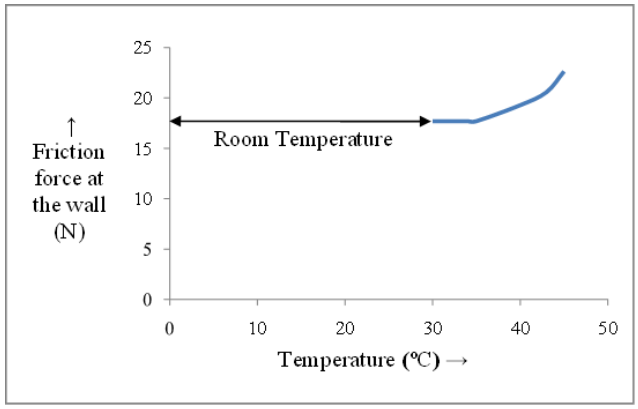

Fig IV.A. vi. (b) Variation of Friction force at the wall with respect to Temperature

Figure IV.A.vi (b) presents the variation of frictional force at the wall for a two-layer fluid system with flow behaviour indices n_1=1.1 and n_2=1.2, inner layer thickness $h_1=3.3333\times10^{-3}$ m and total channel height $h=10\times10^{-3}$ m. The table reports the frictional force F as a function of lubricating oil temperature T_L and the viscosity ratio parameter ε.

It is observed that for temperatures ranging from 30 °C to 35 °C, the frictional force remains constant at 17.68 N when the viscosity ratio is fixed at ε=0.4. This indicates that, within this temperature interval, the combined effect of temperature variation and rheological parameters does not significantly alter the wall shear stress, suggesting a balance between temperature-induced viscosity changes and the imposed flow conditions.

However, at higher temperatures (40–45 °C), an increase in the viscosity ratio parameter (ε=0.6–0.8) leads to a noticeable rise in frictional force from 19.28 N to 22.62 N. This behaviour highlights the dominant influence of viscosity stratification and temperature-dependent rheology on wall shear stress. As the temperature increases, the effective viscosity contrast between the fluid layers is enhanced, resulting in steeper velocity gradients near the wall and consequently higher frictional resistance.

These results demonstrate that, under fixed geometric and rheological indices, the frictional force at the wall is relatively insensitive to moderate temperature variations at constant viscosity ratio but increases significantly when both temperature and viscosity ratio vary simultaneously. This underscores the importance of incorporating temperature-dependent viscosity and layered rheological effects in accurate modelling of peristaltic and lubrication-driven transport systems.

IV.A.vii. Limitation of flux with respect to Amplitude ratio

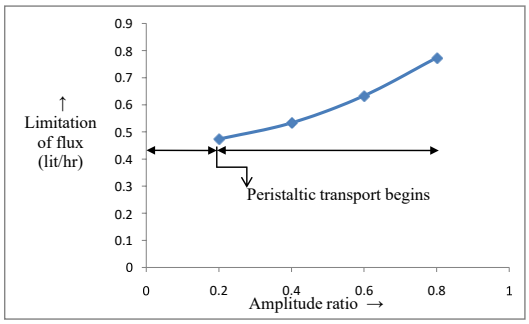

Fig IV.A.vii.: Variation of Limitation of flux with respect to Amplitude ratio

Fig. IV.A.vii. depicts the variation of the limitation of flux with respect to the amplitude ratio of the peristaltic wave. It is observed that the limiting flux increases with an increase in amplitude ratio. Higher amplitude ratios correspond to stronger wall contractions and expansions, which enhance the pumping capability of the peristaltic wave and allow a greater maximum volumetric transport before flow reversal or reflux occurs.

International Journal of Recent Development in Engineering and Technology
Website: www.ijrdet.com (ISSN 2347-6435 (Online) Volume 15, Issue 06, June 2026)

This trend indicates that the amplitude ratio plays a crucial role in determining the upper bound of achievable flux in peristaltic transport, particularly under low Reynolds number conditions where viscous effects dominate.

IV.A,viii. Absolute resistance of flow (R_f)

In the present model, to show the effective positive pumping, the absolute resistance of flow R_f (ratio of average pressure rise to the time average flux) is calculated in the direction of sinusoidal wave

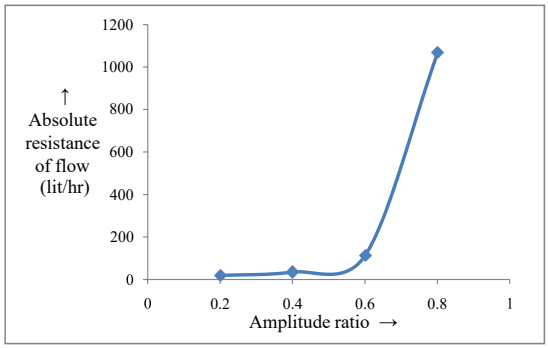

Fig IV.A.viii: Variation of Absolute resistance of flow with respect to Amplitude ratio

Fig. IV.A.viii.. illustrates the variation of the absolute resistance of flow with respect to the amplitude ratio of the peristaltic wave. It is observed that the absolute resistance of flow increases as the amplitude ratio increases. This behavior is attributed to the enhanced wall deformation at higher amplitude ratios, which produces narrower constricted regions within the tube and intensifies viscous dissipation. As a result, greater resistance is offered to the fluid motion, requiring increased pressure to maintain the same flow rate. The figure highlights the strong influence of wave amplitude on flow resistance in peristaltic transport under low Reynolds number conditions.

IV.B Experimental Analysis: **-**

IV.B.i Flow Rate with Motor Speed for Different Fluids

IV.B.i Distilled Water

The variation of flow rate with motor speed for distilled water is illustrated in Fig. IV.B.i.. All experiments were conducted at a constant ambient temperature of 27 °C. The physical properties of distilled water under these conditions are a kinematic viscosity of $\nu = 1.03 \times 10^{-6}$ m²/s and a density of $\rho = 977.77$ kg/m³.

It is evident from Fig. IV.B.i. that the flow rate increases monotonically with increasing motor speed. This behaviour can be attributed to the rise in the frequency of peristaltic waves generated by the rotating rollers, which enhances axial fluid transport along the tube. Since the temperature is maintained constant throughout the experiment, the viscosity remains unchanged. Therefore, the observed increase in flow rate is predominantly governed by the mechanical driving speed of the peristaltic pump. The nearly linear relationship between flow rate and motor speed indicates stable positive displacement pumping characteristics for distilled water under the investigated operating conditions.

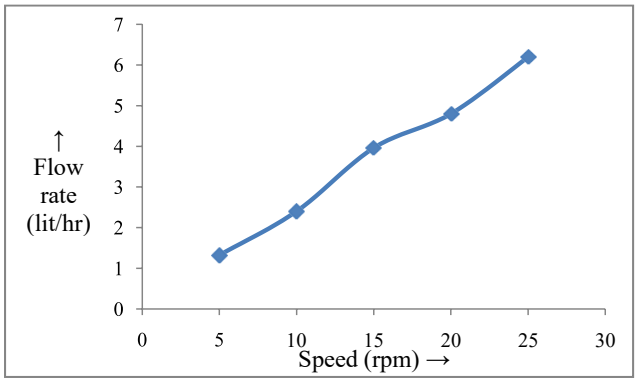

Fig IV.B.i: Variation of Flow rate with Speed of motor for distilled water

IV.B.ii Model Validation with Herschel–Bulkley Fluid Behaviour

The experimental trends shown in Fig. IV.B.ii for lubricating oil SAE 10 further support the applicability of the Herschel–Bulkley fluid model adopted in the theoretical analysis. The monotonic increase in flow rate with motor speed confirms positive peristaltic pumping, while the significantly lower flow rate compared to water highlights the dominant role of viscous and yield-stress effects. In the context of the H–B model, the high effective viscosity corresponds to a lower flow behaviour index and increased resistance to deformation, leading to reduced volumetric transport for a given wave speed. The close qualitative agreement between the experimentally observed flow-rate variation and the analytically predicted flux behaviour validates the suitability of the Herschel–Bulkley formulation for describing peristaltic transport of highly viscous fluids under low Reynolds number conditions.

International Journal of Recent Development in Engineering and Technology
Website: www.ijrdet.com (ISSN 2347-6435 (Online) Volume 15, Issue 06, June 2026)

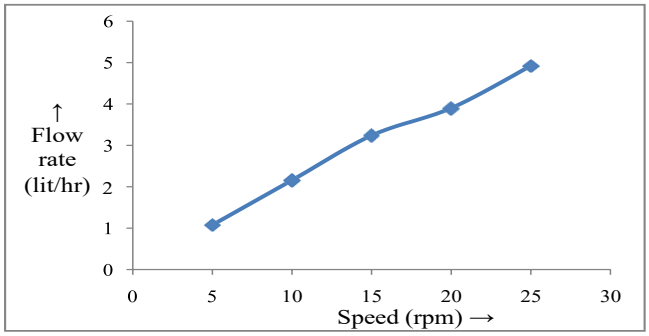

Fig IV.B.ii: Variation of Flow rate with Speed of motor for normal water

IV.B.iii Flow Rate with Motor Speed for SAE 10 Oil

The variation of flow rate with motor speed for lubricating oil SAE 10 is presented in Fig. IV.B.iii. All experiments were conducted at a constant room temperature of 27 °C. The kinematic viscosity and density of SAE 20 oil are $\nu = 166 \times 10^{-6}$ m²/s and $\rho = 872$ kg/m³, respectively.

From Fig. IV.B.iii, it is observed that the flow rate increases with an increase in motor speed, confirming the existence of positive peristaltic pumping. However, for a given motor speed, the flow rate of SAE 20 oil is significantly lower than that of SAE 10 oil. This reduction is attributed to the higher viscosity of SAE 20 oil, which increases viscous resistance and consequently reduces the effective volumetric transport within the peristaltic tube.

These observations emphasize the strong influence of fluid viscosity on peristaltic flow characteristics and demonstrate that, although peristaltic pumps are capable of handling highly viscous fluids, the pumping efficiency decreases with increasing viscosity.

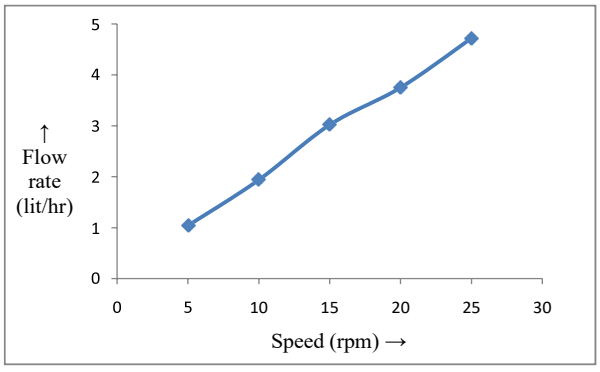

Fig IV.B.iii: Variation of Flow rate with Speed of motor for lubricating oil SAE10

IV.B.iv Flow rate with Speed of motor for lubricating oil SAE 20

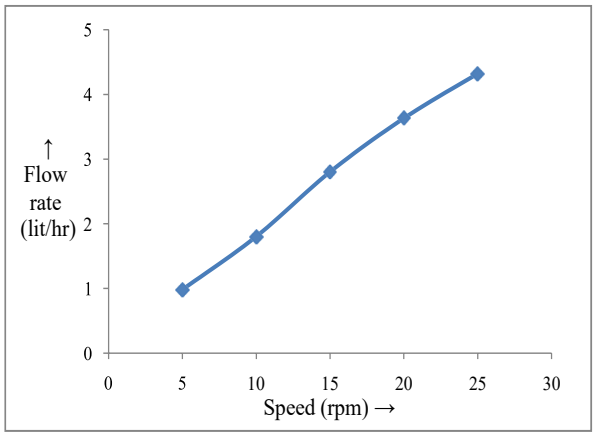

Fig IV.B.iv: Variation of Flow rate with Speed of motor for lubricating oil SAE 20

Fig. IV.B. iv. illustrates the variation of volumetric flow rate with motor speed for lubricating oil SAE 20 at a constant room temperature of 27 °C. The lubricating oil has a kinematic viscosity of $\nu = 166 \times 10^{-6}$ m2/s, and a density of $\rho = 872$ kg/m³. It is observed from the figure that the flow rate of lubricating oil SAE 20 increases monotonically with an increase in motor speed. This behaviour is attributed to the enhanced peristaltic pumping action generated by higher motor speeds, which increases the frequency of wall deformation and consequently augments the forward transport of the highly viscous fluid. Despite the relatively high viscosity of SAE 20 oil, the imposed mechanical driving force dominates viscous resistance, resulting in a steady rise in flow rate under isothermal conditions.

IV.B.v. Flow rate with different viscosity of fluid

The experiment is conducted at a constant motor speed of 18 rpm while varying the working fluid viscosity. The corresponding flow rates are measured for each fluid. From Fig. IV.B.. v**,** it is observed that the flow rate decreases with an increase in fluid viscosity, indicating that higher viscous resistance significantly reduces volumetric transport in peristaltic pumping under identical operating conditions.

International Journal of Recent Development in Engineering and Technology
Website: www.ijrdet.com (ISSN 2347-6435 (Online) Volume 15, Issue 06, June 2026)

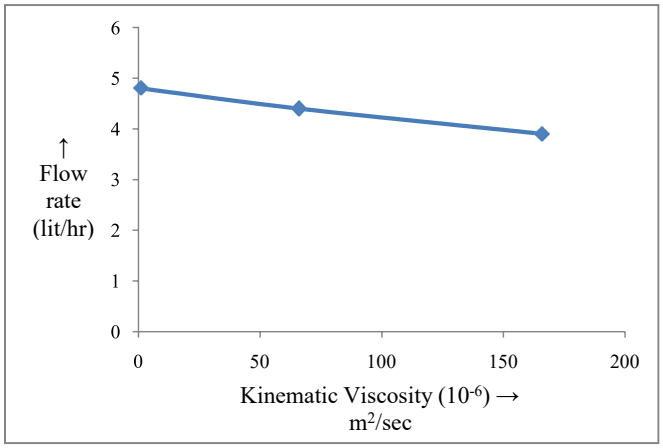

Fig IV.B.v: Variation of Flow rate with different Kinematic viscosity of fluid

IV.B.vi. Flow rate with head of the pump

The experiment is performed by maintaining a constant motor speed of 18 rpm while varying the head of the fluid in the system. The corresponding flow rates are measured for each head. From Fig. IV.B.vi, it is observed that the flow rate decreases with an increase in pump head, due to the rise in opposing pressure which reduces the effective volumetric transport in the peristaltic pumping mechanism.

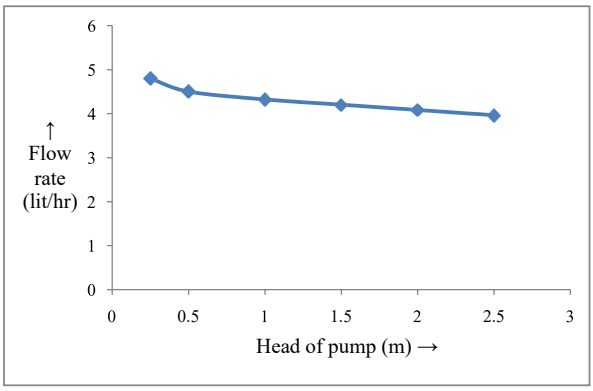

Fig IV.B..vi. Variation of flow rate with head of the pump

IV.C. Experimental flow visualisation of red dye

Fig. IV.C.i. At 27ºC room temperature

Fig.IV.C. ii. At 40ºC heated condition

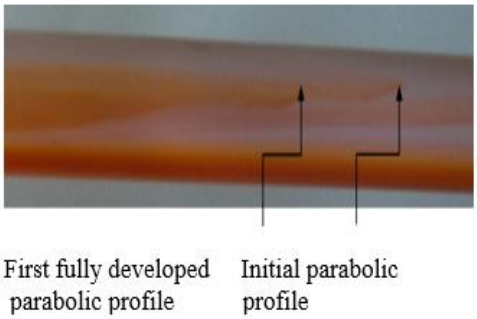

Fig.IV.C.iii. At 45ºC heated condition

Fig.C.(iv) At 50ºC heated condition

Fig IV.C.: Experimental flow visualisation of red dye

- For the experimental fluid (water) with red dye injection at room temperature (Fig. IV.C.i, 27 °C), the velocity profiles obtained from experimental flow visualisation show good agreement with the classical parabolic profile predicted by the Hagen–Poiseuille flow model.

International Journal of Recent Development in Engineering and Technology
Website: www.ijrdet.com (ISSN 2347-6435 (Online) Volume 15, Issue 06, June 2026)

- For the same experimental fluid under heated conditions (Fig. IV.C. ii at 40 °C, Fig. IV.C.iii at 45 °C, and Fig. IV.C.iv at 50 °C), the velocity profiles exhibit increased steepness, corresponding to an extended form of the maximum velocity in axi-symmetric parabolic flow.
- With an increase in the temperature of the experimental fluid, the viscosity decreases, leading to a pronounced steepening of the parabolic velocity profile, which is consistently observed in the experimental flow visualisations.

IV.D. Experimental flow visualisation of blue dye

Fig.IV.D.i. At 27ºC room temperature

Fig.IV.D..ii. At 40ºC heated condition

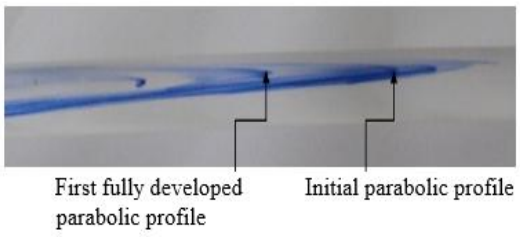

Fig.IV.D iii At 45ºC heated condition

Fig.IV.D.iv. At 50ºC heated condition

Fig IV.D.: Experimental flow visualisation of blue dye

- For the experimental fluid (water) with blue dye injection at room temperature (Fig. IV.D.i, 27 °C), the velocity profiles observed in the experimental flow visualisation closely follow the classical parabolic distribution predicted by the Hagen–Poiseuille flow model.
- Under heated conditions (Fig. IV.D. ii. at 40 °C, Fig. IV.D.iii at 45 °C, and Fig. IV.D. iv. at 50 °C), the velocity profiles obtained with blue dye injection exhibit increased steepness, consistent with an extended parabolic velocity profile for axi-symmetric flow.
- The increase in fluid temperature leads to a reduction in viscosity, which in turn enhances the steepness of the parabolic velocity profile, as clearly reflected in the experimental flow visualisations.

IV.E. Experimental flow visualisation of black dye

Fig.E.i. At 27ºC room temperature

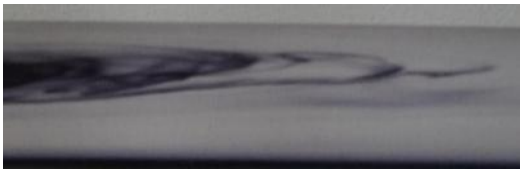

Fig.E.ii. At 40ºC heated condition

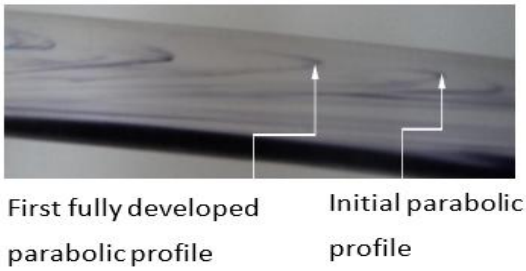

Fig.E.iii. At 45ºC heated condition

International Journal of Recent Development in Engineering and Technology
Website: www.ijrdet.com (ISSN 2347-6435 (Online) Volume 15, Issue 06, June 2026)

Fig.E.iv. At 50ºC heated condition

Fig E. Experimental flow visualisation of black dye

- For the experimental fluid (water) with black dye injection at room temperature (Fig. IV.E.i.), the velocity profiles obtained from experimental flow visualisation are in good agreement with the classical parabolic profile described by the Hagen–Poiseuille flow equation.
- Under heated conditions (Fig. IV.E.ii. at 40 °C, Fig. IV.E.iii at 45 °C, and Fig. IV.E.iv. at 50 °C), the velocity profiles exhibit increased steepness, corresponding to an extended parabolic velocity distribution for axi-symmetric flow.
- As the temperature of the experimental fluid increases, its viscosity decreases, resulting in a more pronounced steepening of the parabolic velocity profile, which is consistently observed in the experimental flow visualisations.

IV.F. Experimental flow visualisation of milk

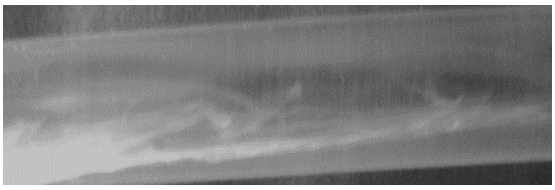

Fig.F.i. At 27ºC room temperature

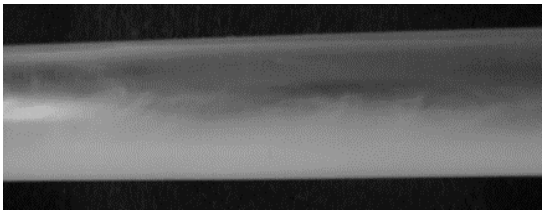

Fig.F.ii. At 40ºC heated condition

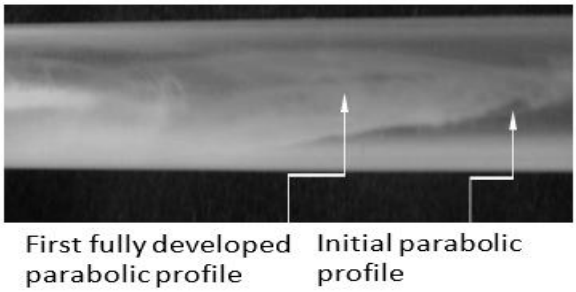

Fig.F.iii. At 45ºC heated condition

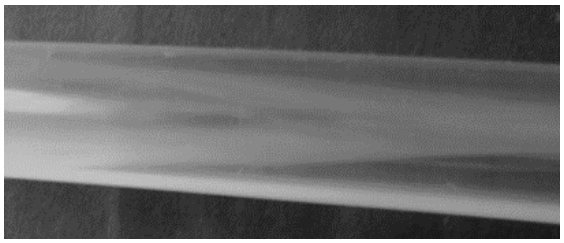

Fig.F.iv. At 50ºC heated condition

Fig IV.F. Experimental flow visualisation of milk

- For the experimental fluid (water) with milk injection at room temperature (Fig. IV.F.i., the velocity profiles observed in the experimental flow visualisation closely match the classical parabolic profile predicted by the Hagen–Poiseuille flow equation.
- Under heated conditions (Fig. IV.F.ii. at 40 °C, Fig. Fig.IV.F.c at 45 °C, and Fig. IV.F.iv. at 50 °C), the velocity profiles show increased steepness, corresponding to an extended parabolic velocity distribution in the axi-symmetric flow regime.
- With increasing temperature, the viscosity of the experimental fluid decreases, leading to enhanced steepness of the parabolic velocity profiles, which is consistently reflected in the experimental flow visualisations.

V. Conclusion

Positive pumping in peristaltic transport has been successfully demonstrated using a two-layer Herschel–Bulkley model fluid framework. The analytical formulation yields parabolic volumetric flux distributions corresponding to two distinct flow behaviour indices (n_i : i =1, i=2) representing the core and peripheral layers.

The obtained results reduce to the classical Hagen–Poiseuille flow solution in the appropriate limiting cases, thereby confirming the mathematical consistency of the developed model.

Experimental flow visualization results corroborate the theoretical predictions. Under room-temperature conditions, velocity profiles exhibit standard parabolic characteristics for all test fluids (red, blue, and black dyes, as well as milk). Under heated conditions, the velocity profiles become steeper due to viscosity reduction. Furthermore, it is observed that increasing fluid viscosity reduces the steepness of the velocity profile, demonstrating the strong dependence of peristaltic transport on rheological properties.

Quantitative evaluation of key peristaltic flow parameters shows close agreement between analytical predictions and experimental observations under both normal and heated conditions, thereby validating the proposed thermo-rheological model. The present investigation establishes a unified analytical–experimental framework for temperature-dependent, two-layer non-Newtonian peristaltic transport. The developed methodology can be extended to physiological flow modelling, microfluidic pumping systems, and bio-inspired transport mechanisms involving complex rheologies and thermal effects.

REFERENCES

[1] A. H. Shapiro, M. Y. Jaffrin, and S. L. Weinberg, "Peristaltic pumping with long wavelengths at low Reynolds number," J. Fluid Mech., vol. 37, no. 4, pp. 799–825, 1969.

[2] Y. C. Fung and C. S. Yih, "Peristaltic transport," J. Appl. Mech., vol. 35, pp. 669–675, 1968.

[3] L. M. Srivastava, V. P. Srivastava, and S. N. Sinha, "Peristaltic transport of a physiological fluid," Biorheology, vol. 20, pp. 153–166, 1983.

[4] A. M. Siddiqui and W. H. Schwarz, "Peristaltic flow of a second-order fluid in tubes," J. Non-Newtonian Fluid Mech., vol. 30, pp. 257–284, 1994.

[5] K. R. Rajagopal and A. S. Gupta, "On peristaltic transport of non-Newtonian fluids," J. Fluid Mech., vol. 109, pp. 417–431, 1981.

[6] K. P. Selverov and H. A. Stone, "Peristaltically driven channel flows," Phys. Fluids, vol. 13, pp. 1837–1859, 2001.

[7] K. Vajravelu, S. Sreenadh, and P. Lakshminarayana, "Heat transfer influence on peristaltic transport," Commun. Nonlinear Sci. Numer. Simul., vol. 16, pp. 3107–3125, 2011.

[8] M. A. Abd-Alla et al., "MHD peristaltic flow of a Jeffery fluid," Sci. Rep., vol. 13, 2023.

[9] N. M. Hafez et al., "Peristaltic transport of second-grade dusty fluid," Sci. Rep., vol. 12, 2022.

[10] M. Rafiq et al., "Activation energy and variable properties in peristaltic flow," Sci. Rep., vol. 13, 2023.

[11] M. Gudekote et al., "MHD peristaltic transport of Eyring–Powell fluid," Arab. J. Sci. Eng., vol. 49, 2024.

[12] S. Nadeem and N. S. Akbar, "Peristaltic transport of nanofluids," Int. J. Heat Mass Transf., vol. 55, pp. 468–475, 2012.

[13] R. Ellahi et al., "Electroosmotic slip in peristaltic transport," Int. J. Heat Mass Transf., vol. 247, 2025.

[14] A. Riaz et al., "Thermal radiation effects on peristaltic nanofluid flow," Phys. Fluids, vol. 32, 2020.

[15] A. Singh and S. R. Shah, "Enhanced pumping of blood flow," Res. Rev. Int. J. Multidiscip., vol. 10, 2025.

[16] R. Vernekar et al., "Hydrodynamics in villi-patterned channel," arXiv, 2025.

[17] F. K. Henn and K. Alim, "Viscosity impact on nutrient uptake," arXiv, 2025.

[18] M. Sohail et al., "Hybrid nanofluid peristaltic transport," Alexandria Eng. J., vol. 62, 2023.

[19] T. Hayat et al., "Peristaltic transport of third-grade nanofluid," Int. Commun. Heat Mass Transf., vol. 124, 2021.

[20] S. Rashidi et al., "Entropy generation in MHD peristaltic nanofluid," Energy, vol. 210, 2020.

[21] H. A. Attia, "Slip effects on peristaltic transport," Appl. Math. Model., vol. 36, 2012.

[22] S. Kothandapani and J. Prakash, "Peristaltic transport in porous channel," Transp. Porous Media, vol. 90, 2011.

[23] S. Sreenadh et al., "Jeffrey fluid peristaltic transport," Nonlinear Anal. Model. Control, vol. 23, 2018.

[24] M. Mustafa et al., "Convective peristaltic nanofluid transport," J. Mol. Liq., vol. 230, 2017.

[25] T. Abbas et al., "Electroosmotic peristaltic nanofluid flow," Phys. Fluids, vol. 33, 2021.

[26] A. Ebaid, "Exact solutions of peristaltic transport," Z. Naturforsch., vol. 63, 2008.

[27] N. Ali and T. Hayat, "Peristaltic flow of Carreau fluid," Physica A, vol. 389, 2010.

[28] M. Shehzad et al., "Nonlinear MHD peristaltic flow," Eur. Phys. J. Plus, vol. 135, 2020.

[29] A. Bhatti et al., "Nanoparticle effects in peristaltic flow," Appl. Math. Mech., vol. 42, 2021.

[30] S. Khan et al., "Thermal dependent viscosity in peristaltic transport," Int. J. Therm. Sci., vol. 171, 2022.

[31] A. Ramesh and P. Devaki, "Two-layer peristaltic transport model," J. Appl. Fluid Mech., vol. 14, 2021.

[32] M. Nadeem et al., "Axisymmetric peristaltic nanofluid transport," Sci. Rep., vol. 14, 2024.

[33] S. Ullah et al., "Hybrid MHD peristaltic nanofluid model," Case Stud. Therm. Eng., vol. 38, 2023.

[34] F. Hussain et al., "Peristaltic transport with radiation and slip," Therm. Sci., vol. 27, 2023.

[35] J. Raza et al., "Temperature-dependent viscosity effects in peristaltic transport," Results Phys., vol. 41, 2022.